The EMBO Journal Vol.17 No.4 pp.945–951, 1998

Proteolytic mapping of kinesin/ncd-microtubule interface: nucleotide-dependent conformational changes in the loops L8 and L12

Maria C.Alonso, Jose van Damme[1], Joel Vandekerckhove[1] and Robert A.Cross[2]

Molecular Motors Group, Marie Curie Research Institute, The Chart, Oxted, Surrey RH8 0TL UK and [1]Flanders Interuniversity Institute for Biotechnology, Department of Biochemistry, Faculty of Medicine, Universiteit Gent, Ledeganck Straat 35, B-9000 Gent, Belgium

[2]Corresponding author
e-mail: r.cross@mcri.ac.uk

We used a battery of proteases to probe the footprint of microtubules on kinesin and ncd, and to search for nucleotide-induced conformational changes in these two oppositely-directed yet homologous molecular motors. Proteolytic cleavage sites were identified by N-terminal microsequencing and electrospray mass spectrometry, and then mapped onto the recently-determined atomic structures of ncd and kinesin. In both kinesin and ncd, microtubule binding shields a set of cleavage sites within or immediately flanking the loops L12, L8 and L11 and, in ncd, the loop L2. Even in the absence of microtubules, exchange of ADP for AMPPNP in the motor active site drives conformational shifts involving these loops. In ncd, a chymotryptic cleavage at Y622 in L12 is protected in the strong binding AMPPNP conformation, but cleaved in the weak binding ADP conformation. In kinesin, a thermolysin cleavage at L154 in L8 is protected in AMPPNP but cleaved in ADP. We speculate that ATP turnover in the active site governs microtubule binding by cyclically retracting or displaying the loops L8 and L12. Curiously, the retracted state of the loops corresponds to microtubule strong binding. Conceivably, nucleotide-dependent display of loops works as a reversible block on strong binding.

Keywords: kinesin/microtubule/molecular motor/ncd/proteolysis

Introduction

The recently solved crystal stuctures of kinesin heavy chain (Kull *et al*., 1996) and its oppositely-directed homologue ncd (Sablin *et al.*, 1996) revealed extensive structural similarities between the two molecules and also clear structural homology to the catalytic core of myosin and the RAS family of GTPases (Vale, 1996). The structural similarity suggests that the active sites of kinesin and ncd may undergo conformational changes, homologous to those that occur in RAS and myosin, particularly in response to the presence or absence of the gamma phosphate of ATP (Vale, 1996). How these putative motions in the motor active site are amplified globally in order to step the motor along the microtubule is, however, unknown. The mechanism of this so-called mechano-chemical coupling is the major problem in the field. We describe here the use of a proteolytic version of the well-known DNA footprinting technique, to probe for nucleotide-induced conformational changes in kinesin and ncd, and to map the microtubule contact surfaces for the two motors in different nucleotides. The results support the conclusions of a recent alanine scanning study of the microtubule-binding face of kinesin (Woehlke *et al.*, 1997). Our data extend the earlier work by providing information about the solvent-exposed face of kinesin, about both faces of ncd, and about nucleotide-dependent conformational effects at the microtubule recognition interfaces of both motors.

Results

The data are summarized in Table I. The dataset comprises 18 cleavage sites in kinesin and 19 in ncd. Digestions were made over a three-decades concentration range of each protease, in the presence and absence of superstoichiometric concentrations of microtubules, and in the presence of Mg-ADP or Mg-AMPPNP. Motor-ADP is a weakly microtubule-binding species (K_d ~10–20 μM) and motor-AMPPNP is a strongly microtubule-binding species (K_d <1 μM; Amos and Cross, 1997). Cleavage patterns were visualized using SDS gradient gel electrophoresis. Digestion products were analysed only in cases where the pattern of peptide products of digestion was simple. With respect to these first few cleavages, the protease acts as a probe of the native conformation. Clearly, at later stages of digestion, the protease is cutting an already cleaved protein, whose conformation may well differ from that of the native protein. We screened the proteases trypsin, chymotrypsin, papain, V8 (Glu-C), Arg-C, Lys-C, thrombin, proteinase K and thermolysin. Cleavage products were initially identified by N-terminal microsequencing of bands from electroblots. C-termini were subsequently identified by electrospray mass spectrometry of peaks from HPLC-fractionated digests and further, confirmatory, N-terminal sequencing.

The spatial distribution of proteolytically susceptible sites was broadly similar for ncd and kinesin; most cuts were in surface loops which project from the core structures. Cleavages which were present in one protein and not in the other were usually due simply to the absence of an equivalent proteolytically susceptible residue in the uncut species.

There are two levels of information in the cleavage site data. First, they identify residues on ncd and kinesin which are exposed to protease attack in the absence of microtubules, and protected in the presence of microtubules. This protected set of cleavages comprises a map of the occluded microtubule–motor interaction surface. Second, the data identify residues that move in response

Table I.

Cleaved residue		Protease	Structural element	Protected (P) or unprotected (NP)
Rat KΔ340	Human equivalent			In ADP
E37	D37	V8 (Glu-C)	β1b	NP
Y47	Y46	chymotrypsin	β1c	NP
I70	I69	thermolysin	α1 middle	P[a]
F83	F82	chymotrypsin	β3 middle	NP
K151	K150	trypsin	L8 middle	P
L154	L153	thermolysin	β5a start	P[a]
E158	E157	V8 (Glu-C)	β5a end–L8	NP
Y165	Y164	chymotrypsin	β5b	NP
K188	K187	Lys-C	α3	NP
Y229	Y228	chymotrypsin	β7	NP
K241	K240	trypsin	β7a start	P
E245	E244	V8 (Glu-C)	L11	[P]
A247	A246	protease K	L11	[P]
L249	L248	protease K	L11	[P]
K253	K251	Lys-C; trypsin	β7b	P
I255	I253	thermolysin	β7b	P
K257	K256	trypsin; Lys-C	α4	P
K274	K273	trypsin; Lys-C	L12	P
Drosophila NΔ333–700				
W370		chymotrypsin	β1a	NP
E379		V8 (Glu-C)	β1b	NP
Y442		chymotrypsin	α2	NP
E449		V8 (Glu-C)	L5 middle	NP
K498		trypsin	L8 middle	NP
E501		V8 (Glu-C)	β5a start	NP
E519		V8 (Glu-C)	β5c	NP
E520		V8 (Glu-C)	β5c	NP
V522		V8 (Glu-C)	β5c end	NP
R539		Arg-C	L9 start	NP
K388		trypsin; Lys-C	L2 middle	[P]
K390		trypsin; Lys-C	L2 middle	[P]
M500		thermolysin	end β5a	P
K506		V8 (Glu-C)	L8	[P]
R592		trypsin; Arg-C	β7a / L11	P
E595		V8 (Glu-C)	L11	P
I599		thermolysin	end 7b	P
L603		thermolysin	α4	P
Y622		chymotrypsin	L12	P[a]

Summary of cleavage data. The X-ray structure (Figure 1) is of human kinesin, and the slightly different numbering of rat kinesin is shown for comparison. Cleavage sites identified by the sequencing studies are classified as either completely protected (P) or unprotected (NP). Square brackets indicate partial protection. Protection against cleavage was in all cases induced by AMPPNP.
[a] indicates AMPPNP-induced protection in the absence of MTs.

to nucleotide binding in the active site. Some cleavages are unavailable in one nucleotide and available in the other, even in the absence of microtubules. These latter data identify proteolytic signatures of the ADP-induced (weak binding) and AMPPNP-induced (strong binding) conformations of the two motors, and represent the first strong evidence for significant nucleotide-dependent domain motions within the kinesin–ncd head.

Microtubule-binding footprint on ncd and kinesin

Figure 1 shows space filling views of the putative solvent-exposed and putatively microtubule-shielded faces of the crystal structures of ncd-ADP (Sablin *et al*., 1996) and kinesin-ADP (Kull *et al*., 1996). The views of ncd and kinesin are approximately equivalent in orientation. Residues that are protected from cleavage by microtubule binding are highlighted in yellow, those cleaved microtubule-independently in purple, and those cleaved nucleotide-dependently in the absence of microtubules in green.

For kinesin, protection is apparent within the loop L8–sheet 5a (K150) complex, within the L12 loop (K274), within the β7a (K240)- and β7b (K253, I254)-sheets which flank the L11 loop, within the L11 loop itself (E245,A247,L249) and within the adjacent helix α4 (K256). These sites fall within two contiguous stretches of the primary sequence and correspond to distinct patches on the putative microtubule-binding surface of the motor (Woehlke *et al*., 1997).

For ncd, protection occurs analogously in the 5a–L8 complex (M500, K505), in the sheet 7a–loop L11–sheet 7b complex (R592, E595, I599) and in α4 / L12 (L603, Y622). Additionally, protected sites occur in the loop L2 (K388, K390), which is vestigial in kinesin. ncd thus appears to have an extra contact with the microtubule surface over and above those made by kinesin.

In both kinesin and ncd, the loop L11 is protected on both its front and back faces. This suggests that it may fit into a socket in the microtubule, possibly wedging between

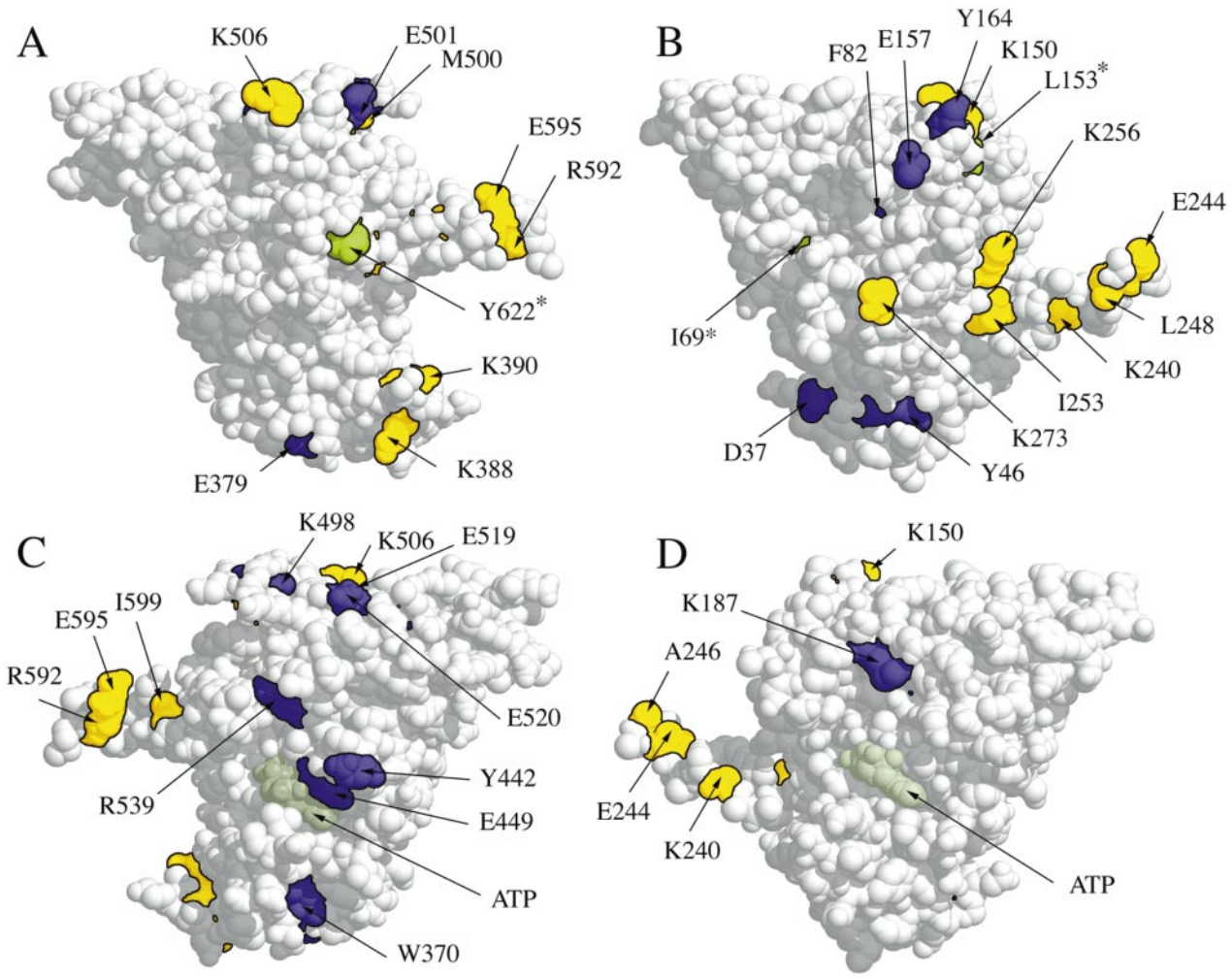

Fig. 1. Cleavage maps. Space filling views of the ncd (**A** and **C**) and kinesin (**B** and **D**) molecules viewed from the putative microtubule-binding (A and B) and exposed (C and D) faces. Sites that are proteolytically cleaved in the presence or absence of microtubules are shown in purple. Sites cleaved only in the absence of microtubules are shown in yellow. Sites shown in green and marked with an asterisk are protected by exchanging active site ADP for AMPPNP, even in the absence of microtubules.

two protofilaments as suggested by modelling (Sosa *et al.*, 1997). Something similar must happen with kinesin, but it is difficult to draw definitive conclusions because the L11 loop is invisible (and therefore mobile) in the kinesin-ADP X-ray map.

Cleavages that were not protected by nucleotide or microtubules

Unprotected sites on both proteins mark exposed surfaces to which the proteases (which are around half the size of the motor) can gain access. The solvent-exposed surface is defined best by the ncd data. Kinesin contains few susceptible sites on the equivalent surface. Five residues (K498, E520, R539, E449, W370) spread across the exposed surface of ncd are cleaved in either ADP or AMPPNP, and in the presence or absence of microtubules. The kinesin dataset has only one cleavage on this putatively solvent-exposed surface (K187 in helix α3). Protease-accessible sites appear in Figure 2 to invade some parts of the microtubule-binding face of kinesin. However, this is illusory. The protected sites (in yellow) can be seen in appropriate views (not shown) to form a projecting ridge of density, with the cleavable sites accessible on either side. The fit of this surface to the microtubule must preserve the accessibility of these residues on either side of the ridge.

Based on these data, we assigned the microtubule-binding and exposed faces of ncd and kinesin. The assignment is as expected based on the position of the conserved putatively microtubule-binding loop L12, and consonant with assignments made recently for kinesin on the basis of alanine scanning mutagenesis of the putative microtubule-binding face of the molecule (Woehlke *et al.* 1997) and by fitting by eye of the the ncd-ADP crystal structure into cryoEM 3D reconstructions of ncd-AMPPNP heads bound to microtubules (Sosa *et al.*, 1997). The microtubule interface of kinesin comprises the loops L8, L11 and L12. That of ncd comprises the same set of loops, but we detected an additional contact involving L2.

Cleavages that were sensitive to nucleotide in the absence of microtubules

Importantly, some cleavages were nucleotide-sensitive in the absence of microtubules. In these cases, the proteases are sensing nucleotide-induced conformational shifts. In kinesin, we detected in this way motion at L154, a thermolysin cleavage at the start of sheet 5a within the L8 complex and at I70, which lies in the middle of the

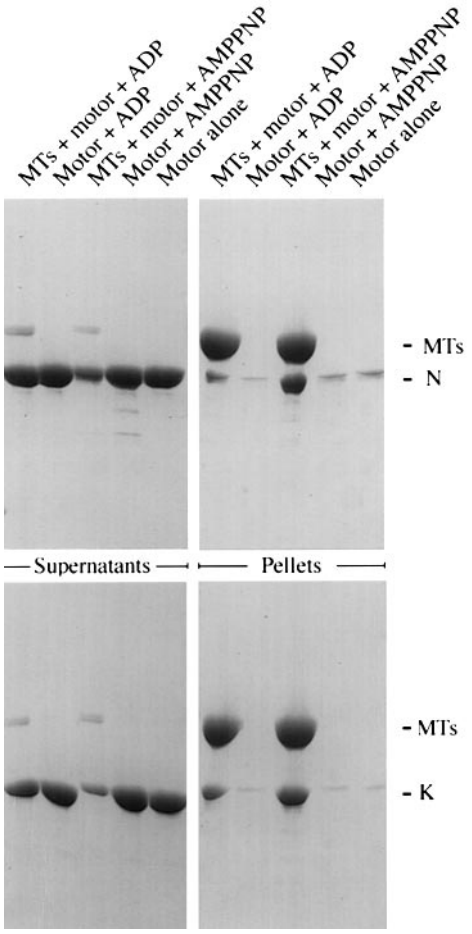

Fig. 2. Protein purity and binding controls. Supernatants and pellets following ultracentrifugation (10 min, 130 000 *g*) are shown at equivalent loadings. ADP-containing kinesin or ncd is substantially dissociated from microtubules under the conditions of these experiments. AMPPNP drives near-quantitative association. Additional controls show negligible pelletting of the expressed motors in the absence of microtubules.

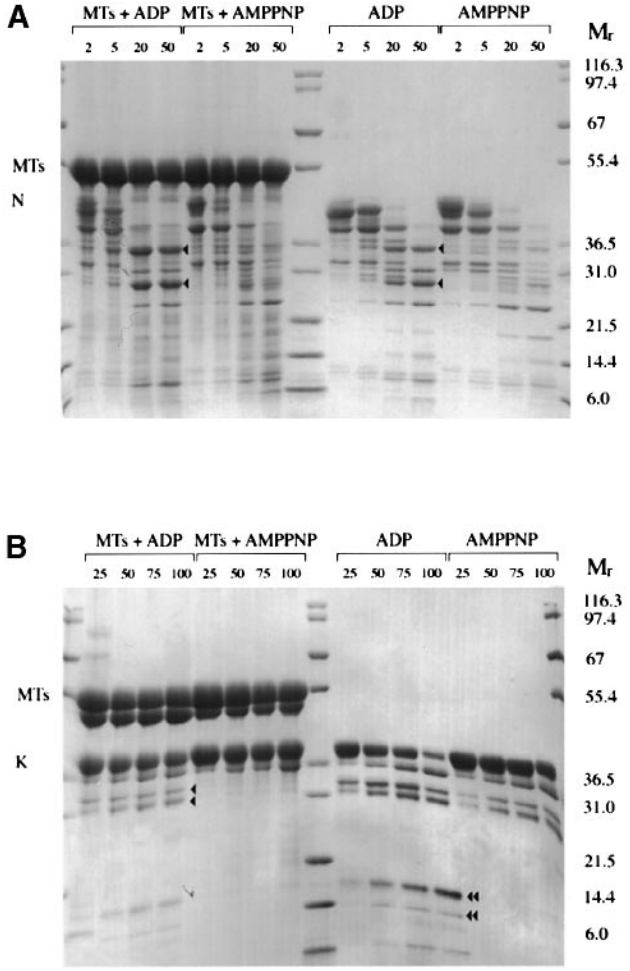

Fig. 3. (**A**) Chymotrypsin cleavage patterns of the ncd construct Nδ333–700 in ADP or AMPPNP in the presence or absence of microtubules. The bands marked are only generated when ADP is in the active site. They arise by cleavage at the tyrosine of the conserved HYPR sequence in L12 (see text). The far left, centre and far right tracks are molecular weight markers as shown. The numbering of the tracks corresponds to the protease concentration in μg/ml.
(**B**) Thermolysin cleavage of the kinesin construct KΔ340 in ADP or AMPPNP in the presence or absence of microtubules. Formation of the bands marked with a double chevron require ADP to be in the active site. Formation of the bands marked with a single chevron is blocked in microtubules plus AMPPNP but not in any other condition.

helix A1. In ncd, nucleotide-dependent cleavages were detected in Y622, the Y in the conserved HY/VPR sequence which forms the L12 loop. The nucleotide-dependent cleavage at I70 in α1 of kinesin suggests a nucleotide-dependent breathing motion there also. I70 is distant from the microtubule-interacting loops, but close to the N-terminus.

Additionally, we note that in the kinesin map, K150 in L8 is protected by microtubule binding, yet K166, which lies on top of it, is not. This strongly suggests that K150 is protected by an indirect mechanism and microtubule binding induces a conformational change which acts to bury K150. Parallel behaviour was observed for ncd: M500 in L8 of ncd is protected by microtubule binding, but E501, which overlies it, is not. Again, this suggest that microtubule tight binding induces a conformational shift, altering the relationship of this pair of residues, such that M500 becomes buried. K150 and M500 are in analogous positions in the homologous structures of ncd and kinesin, at the end of sheet B5a in L8.

These nucleotide- and microtubule-dependent cleavages are the first strong evidence for substantial domain motions with the kinesin–ncd head, and provide diagnostic proteolytic fingerprints for the ADP (weak binding) andAMPPNP (strong binding) conformational states of the motors. The data suggest that nucleotides may control microtubule affinity of the motors by deploying or retracting (or changing the interdistance between) microtubule-binding loops (see Discussion).

Discussion

Strengths and limitations of the protein footprinting approach

Proteolytic cleavage is a traditional method for obtaining conformational information about native proteins in solution, and has been used extensively and succesfully in the motors field to detect changes in myosin conformation. However, this work was done at a time when it was impracticable to determine more than a few cleavage sites by sequencing. Using microsequencing and electrospray

mass spectrometry, it is now feasible to do extensive mapping of interfaces and conformation using proteolysis and, as we have shown here, the method can be a useful compliment to directed mutagenesis in determining protein–protein interaction surfaces. Its merits are that it deals with the native protein rather than with a mutant and that it yields information about conformational changes as well as interaction surfaces. The demerits of proteases as structural probes stem from their large size relative to the protein of interest, from a lack of 'restriction proteases' and from uncertainties over the conformational effects of the cleavages themselves on subsequent cleavages. It may be that its best use is to yield, as here, a 'big picture' on binding surfaces and conformational changes, which can then be refined using single-residue mutagenesis.

ncd and kinesin bind congruently, but there are some differences

It is clear that, as expected, microtubules bind to ncd and kinesin so as to protect the loops L12, L11 and L8 from proteolytic cleavage. Possible differences in the binding interfaces of kinesin and ncd are of interest because they may relate to the opposite directionality of these proteins. There are two cleavages which hint at differences in the contact interface for ncd versus kinesin. First, in ncd the loop L2 is protected by microtubules, suggesting it forms part of the interface. This loop is vestigial in kinesin. Second, K506 of ncd, at the end of β-sheet 5a in the L8 complex, is protected by microtubule binding, while E156 (E157 in human) at an approximately equivalent position in the kinesin primary structure is not.

Nucleotide-dependent conformational changes in the L8 and L11 loops, even in the absence of microtubules

Aside from mapping contact surfaces, protease cleavage can also yield conformational information. The current data show that the loops L12 and L8 can be cleaved when ADP is in the active site but are protected when AMPPNP is in the active site. These data are the first direct evidence for nucleotide-induced conformational rearrangements involving the L8 and L12 loops. These two loops had been expected to bind microtubules based on sequence comparisons with myosin: the L8 and L12 loops in kinesin–ncd correspond to the sites of presumed insertions in the catalytic core of a common ancestor of myosins and kinesins. The corresponding myosin loops bind actin. As discussed by Woehlke *et al.* (1997), an involvement of the L12 loop particularly in microtubule binding was expected based on earlier deletion mutagenesis work by Yang *et al.* (1989), which showed also that the first 130 residues of kinesin were not required for microtubule binding.

Implications for the mechanism of motility: support for a two-state model

We have previously argued the merits of a two-state model for kinesin–ncd mechanism, in which mechanochemical coupling, the coupling of active site chemistry to the mechanical action of the motor, hinges on the nucleotide-dependent switching of the motor into and out of the weakly microtubule-binding trapped ADP conformational state (Lockhart and Cross, 1994; Amos and Cross, 1997). The current data provide robust support for this view, by establishing that distinct global structural states correspond to the switch between the 'trapped' ADP state and the 'open' AMPPNP states. Switching the active site nucleotide from ADP to AMPPNP drives a conformational shift which involves the retraction or display of the loops L12 and L8, which are on the opposite face of the molecule to the nucleotide binding site. Based on the alanine scan performed on kinesin by Sosa *et al.* (1997), and on the current data on both kinesin and ncd, it is likely that L12 and L8 bind direct to microtubules. We speculate, therefore, that the phosphate sensor mechanism (Vale, 1996) in the active site governs microtubule binding by cyclically retracting or displaying the loops L8 and L12. Curiously, the microtubule strong binding (motor-AMPPNP) conformation of kinesin–ncd is the one in which the L12 and L8 loops are protected from cleavage, suggesting that in their strong-binding (force-holding) conformation, the loops are retracted against the surface of the molecule. The possibility arises that these loops mediate the initial, weak binding interaction of motor with the microtubule surface, and must retract before strong binding, involving more extensive contact, can occur; in other words, the function of one or both of the loops L8 and L12 is to reversibly block strong binding. Future experimental work will aim to illuminate more fully the protein-mechanical pathway by which nucleotide turnover in the active site cyclically reconfigures the microtubule-binding interface, and mechanical tension on the motor conversely modifies the active site chemistry.

Materials and methods

Construction of Nδ333–700

Nδ333–700 was constructed using an insert derived from the clone 1a (Endow *et al*., 1990) by PCR, using primers 5′ c ttc cag tcg cat atg gag cgc aaa gag c 3′ and 5′ gg ctc aga atg aat tct tta ttt atc gaa att gcc gc 3′. The PCR product was digested with *Eco*R1 and *Nde*1 and the cleaved product purified and ligated into pET17b, cleaved with the same enzymes.

Expression and purification of Nδ333–700

Expression was performed in BL21(DE3) cells freshly transformed with p1103NRncdET plasmid. Overnight cultures of bacteria were diluted 1 in 50 into 2×YT medium supplemented with ampicillin at 100 μg/ml and grown with shaking at 37°C until the absorbance at 600 nm was 1.0. The cells were shaken for a further 30 min at 22°C before induction with IPTG at 0.2 mg/ml and after a further 6 h shaking at 22°C, the bacteria were harvested by centrifugation. The cell pellets were frozen in liquid nitrogen and stored at –70°C.

Cell pellets of ~60 g were resuspended using a hand held Braun homogeiniser in buffer P (20 mM Na_2HPO_4 - NaH_2PO_4 pH 7.4, 1mM DTT, 2 mM $MgCl_2$) at 1 g/3 ml,, supplemented with complete protease inhibitor cocktail tablets (Boehringer) at the recommended dosage and incubated on ice with lysozyme (0.1 mg/ml) and triton X–100 (0.05%) for 20 min. The cell lysate was supplemented with $MgCl_2$ to 10 mM and DNAase to 40 μg/ml and incubated for a further 15 min on ice. The supernatant was clarified by centrifugation 33 646 *g* at 4°C for 40 min and the cell pellet discarded.

All chromatography steps were pefomed using an FPLC system (Pharmacia Biotech, St Albans UK) at 4°C. Nδ333–700 was purified by passing the clarified supernatant after dilution with buffer P over a 20 ml HiTrap SP column (Pharmacia) equilibrated with buffer P. The column was washed until a stable baseline was achieved, and the bound protein then eluted using a step-increase in salt to 100 mM NaCl in buffer P. Fractions were analysed for purity using SDS microslab gel electrophoresis, and the peak fractions pooled. The pool was supplemented with 20% glycerol, aliquoted, flash frozen in, and stored under, liquid nitrogen. Once thawed, the protein was used immediately. Dilutions of the protein were made in BRB80. Protein concentrations were set based on measured

absorbances at 280 nm, using extinction coefficients calculated from the tryptophan and tyrosine content of the proteins, using values of 5690/M/cm for tryptophan and 1280/M/cm for tyrosine (Gilbert and Johnson, 1993), and incorporating an allowance of 2500/M/cm for copurifying stoichiometric ADP. The values were 15 300/M/cm for K340 and 29 000/M/cm for Nδ333–700.

Construction of K340

The construction of K340 was as described in Lockhart *et al.* (1995).

Expression and purification of K340

Expression and purification of K340 were as for Nδ333–700 except that cells were harvested after only 4 h at 22°C following induction. Cells were resuspended in PIPES buffer (20 mM PIPES pH 6.9, 1 mM DTT, 2 mM $MgCl_2$). Protein was eluted from the 10 ml HiTrap-SP column using 0.1 M NaCl in PIPES buffer. Pooled peak fractions were loaded onto a 1 ml HiTrap Q (Pharmacia) column equilibrated with 0.1 M NaCl PIPES buffer. Protein was eluted with 0.2 M NaCl PIPES buffer, fractions analysed for purity by SDS–PAGE, supplemented with 20% glycerol, aliquoted, flash frozen in, and stored under, liquid nitrogen.

Microtubules

Tubulin was purified from porcine brain as described in Lockhart and Cross (1994). Tubulin (typically 5 mg/ml in 50 mM PIPES pH 6.9, 1 mM EGTA, 0.2 mM $MgCl_2$, 0.01 mM GTP and 20% glycerol) was polymerised by the addition of $MgCl_2$ and GTP to final concentrations of 2 mM and 1 mM, respectively. The tubulin was incubated for 30 min at 37°C, at which point paclitaxel (taxol) was added to a final concentration of 20 μM. In order to remove guanine nucleotides the taxol stabilised microtubules were pelleted by centrifugation (100 000 *g*, 10 min, 25°C). The supernatant was removed and the microtubule pellet carefully resuspended in buffer (80 mM PIPES pH 6.9, 1 mM $MgCl_2$, 1 mM EGTA and 20 μM taxol). Microtubule concentrations were determined spectrophotometrically following this washing, using a value of 55 000/M/cm, and are expressed per tubulin heterodimer.

Proteolytic digests

Proteases were sequencing grade from Boehringer (Mannheim). Protease concentrations were set to levels at which motors were cut but microtubules were not, as judged by SDS electrophoresis. A C-terminal peptide may have been lost from the microtubules. Cleavage of this peptide was previously shown to have no influence on kinesin driven microtubule motility or ATPase (Marya *et al.*, 1994), although a C-terminal tubulin peptide can be cross-linked to kinesin (Tucker and Goldstein, 1997) and so may interact with the motor. We made test digestions using chymotrypsin, trypsin, papain, V8, Lys-C, Arg-C, thrombin, thermolysin and proteinase K in a BRB80 buffer, modified as necessary. With each, we compared the motor digestion patterns in 2 mM ADP with those in 2 mM AMPPNP in the presence and absence of microtubules. Nucleotide concentrations were set to 2 mM, which is ~4-fold higher than the K_m for AMPPNP (Crevel *et al.*, 1996). Note that AMPPNP is reported to be a substrate for ncd (Suzuki *et al.*, 1997). Microtubule concentration was set to 16 μM (heterodimers), and motor concentration to 8 μM, so as to substantially populate the microtubule-bound states. Digestions were made at 25°C in a dry bath, over a three-decade range of protease concentration. Reactions were stopped by addition of hot SDS sample mix and immediately boiled for 5 min. Microtubule preparations were stabilised with taxol and rinsed twice to remove GTP and GDP. The microtubules were disperse when diluted and viewed by computer enhanced DIC microscopy (not shown) and were pelletted essentially quantitatively by 10 min ultracentrifugation at 22°C and 109 000 *g*. Both motors remained >98% in the supernatant in the absence of microtubules under these conditions, but pelletted ~70% with the microtubules in the presence of AMPPNP, and ~15% with microtubules in the presence of ADP. These binding controls are shown in Figure 2.

Polypeptide separation, NH2-terminal sequencing and mass determination

We sought to analyse only those digests that yielded relatively simple patterns of cleavage products, in which we could clearly discern which cleavage products were differentially protected by different nucleotides and/or microtubules. 10–20% SDS microslab gel electrophoresis and blotting on to PVDF membranes (Immobilon-P; Amersham) for N-terminal microsequencing was according to Matsudaira (1993). N-terminal sequences of cleavage products were determined initially by N-terminal microsequencing from Electroblots. C-terminal sequences were determined by HPLC fractionation of the digestion mixtures followed by on-line electrospray mass spectrometry. The identity of the HPLC peaks was reconfirmed by N-terminal sequencing, as follows. Protein fragments, generated by limited and controlled cleavage (as described above) were separated by reversed-phase HPLC on a C4 I.D., 2.1×50mm column (p/n 214TP5205, Vydac Separation Group Hesperia CA) using a 130A HPLC solvent delivery system (Applied Biosystems, Perkin Elmer). Solvent A was 0.1% trifluoroacetic acid (TFA) in water, while solvent B consisted of 0.09% TFA in water mixed with an isopropanol acetonitrile mixture (4:6) in a ratio 5:95 (by volume). A linear gradient from 5% B to 60% B in 90 min was generated at a flow of 80 μl/min at 50°C. Eluting polypeptides were detected by U.V. absorbancy at 214 nm. Peaks were collected manually in Eppendorf tubes and aliquots were taken for automated NH_2-terminal sequence analysis using a pulsed-liquid sequenator model 477A equipped with a 120A phenylthiohydantoin amino acid analyser.

The column eluate was separated with a flow splitter device directing 80% of the eluate into the UV detector and 20% into the ionisation chamber of a single quadrupole mass spectrometer (model Platform, Micromass, Manchester, UK). The instrument was equipped with an electrospray ion source and the m/z ratios were measured using a quadrupole analyser. The flow rate of the peptide carrier solvent at the inlet was ~16 l/min. Droplet evaporation was achieved by heating the ion source at 60°C and with a stream of N_2 gas at about 200 l/h. The mass spectrometer was scanned over m/z values ranging from 450 to 1550 at a rate of one scan every 7 s. Data acquisition was done in the centroid mode. The instrument was calibrated with sodium iodide and controlled for data acquisition and data analysis with the Masslynx-software, version 2.0 (Micromass)

Acknowledgements

We thank John Kull very much for generously providing the kinesin and ncd coordinates, and Marc Goethals for expert sequencing work. We would also like to thank Scott Brady for the rat KHC clone, Sharyn Endow for the drosophila ncd clone, Andrew Lockhart for preparing the K340 construct, Isabelle Crevel for tubulin, Ramiro Fernandez Franco for pilot experiments and Linda Amos for moral support and helpful advice. Work in the Vandekerckhove lab was supported by EC grant ERB CHRX-CT94–0430 and by a grant from Concerted Research Action (GOA). This paper is dedicated with affection and gratitude to the memory of Carlos V.Cabrera.

References

Amos,L.A. and Cross,R.A. (1997) Structure and dynamics of molecular motors. *Curr. Opin. Struct. Biol.*, **7**, 239–46.

Crevel,I.M.-T.C., Lockhart,A. and Cross,R.A. (1996) Weak and strong states of kinesin and ncd. *J. Mol. Biol.*, **257**, 66–76.

Endow,S.A., Henikoff,S. and Soler-Niedziela,L. (1990) Mediation of meiotic and early mitotic chromosome segregation in drosophila by a protein related to kinesin. *Nature*, **345**, 81–83.

Kull,F.J., Sablin,E.P., Lau,R., Fletterick,R.J. and Vale,R.D. (1996) Crystal structure of the kinesin motor domain reveals a structural similarity to myosin. *Nature*, **380**, 550–555.

Gilbert,S.P. and Johnson,K.A. (1993) Expression, purification, and characterization of the Drosophila kinesin motor domain produced in *Escherichia coli*. *Biochemistry*, **32**, 4677–4684.

Lockhart,A. and Cross,R.A. (1994) Origins of reversed directionality in the ncd molecular motor. *EMBO J.*, **13**, 751–757.

Lockhart,A., Crevel,I.M.-T.C. and Cross,R.A. (1995) Kinesin and ncd bind through a single head to microtubules and compete for a shared MT binding site. *J. Mol. Biol.*, **249**, 763–771.

Marya,P.K., Syed,Z., Fraylich,P.E. and Eagles,P.A. (1994) Studies using a fluorescent analogue of kinesin. *J. Cell Sci.*, **107**, 399–44.

Matsudaira,P. (1993) *A Practical Guide to Protein and Peptide Purification for Microsequencing*. 2nd edition, Academic Press.

Sablin,E.P., Kull,F.J., Cooke,R., Vale,R.D. and Fletterick,R.J. (1996) Crystal structure of the motor domain of the kinesin-related motor ncd. *Nature*, **380**, 555–559.

Sosa,H., Prabha Dias,D., Hoenger,A., Whittaker,M., Wilson-Kubalek,E., Sablin,E., Fletterick,R.J., Vale,R.D. and Milligan,R.A. (1997) A model for the microtubule–ncd motor protein complex obtained by electron microscopy and image analysis. *Cell*, **90**, 217–224.

Suzuki,Y., Shimizu,T., Morii,H. and Tanokura,M. (1997) AMPPNP is a substrate for kinesin. *FEBS Lett*, **409**, 29–32.

Tucker,C. and Goldstein,L.S.B. (1997) Probing the kinesin-microtubule interaction. *J. Biol. Chem.*, **272**, 9481–9488.
Vale,R.D. (1996) Switches, latches, and amplifiers: common themes of G proteins and molecular motors. *J. Cell. Biol.*, **135**, 291–302.
Woehlke,G., Ruby,A.K., Hart,C.L., Ly,B., Hom-Booher,N. and Vale,R.D. (1997) Microtubule interaction site of the kinesin motor. *Cell*, **90**, 207–216.
Yang,J.T., Laymon,R.A. and Goldstein,L.S. (1989) A three-domain structure of kinesin heavy chain revealed by DNA sequence and microtubule binding analyses. *Cell*, **56**, 879–889.

Received October 14, 1997; revised and accepted December 4, 1997